

Planetary system, star formation, and black hole science with non-redundant masking on space telescopes

Anand Sivaramakrishnan¹ (AMNH), Peter Tuthill (U. Sydney), Frantz Martinache (Subaru),
Michael Ireland (U. Sydney), James Lloyd (Cornell), Marshall Perrin (UCLA),
Rémi Soummer (STScI), Barry McKernan and Saavik Ford (CUNY)

ABSTRACT

Non-redundant masking (NRM) is a high contrast, high resolution technique relevant to future space missions concerned with extrasolar planetary system and star formation, as well as general high angular resolution galactic and extragalactic astronomy. NRM enables the highest angular resolution science possible given the telescope's diameter and operating wavelength. It also provides precise information on a telescope's optical state. NRM relies on its high quality self-calibration properties and the robustness of interferometric techniques, whereas coronagraphy requires exquisite wavefront quality. Stability *during* an observation sets fundamental NRM contrast limits. A non-redundant mask was recently added to JWST's Fine Guidance Sensor Tunable Filter Imager (FGS-TFI) instrument, bringing a no-cost, no-impact boost in angular resolution that complements JWST's coronagraphs. The JWST NRM search space lies between 50 and 400 mas at 3.8 to 5 μm , even if the telescope's image quality does not meet requirements. JWST's NRM will produce 10 magnitudes of contrast in a 10 ks exposure on an M=7 star, placing Taurus protoplanets and nearby Jovians younger than 300 Myr within JWST's reach.

Future space telescopes can improve vastly on JWST's NRM by utilizing more refined observing methods, and instrumentation designed to take full advantage of NRM's high dynamic range. The ATLAST 16 m design can deliver 10 to 12 magnitudes of contrast between 0.7 to 6 mas at 0.1 μm . On an 8 m telescope at 0.1 μm NRM resolution is almost ten times finer than ALMA's finest resolution. Polarization with space-based NRM opens new vistas of astrophysics in planetary system and star formation as well as AGNs and structure around galactic black hole candidates. Space NRM explores areas inaccessible to both JWST coronagraphs and future 30-m class ground-based telescopes. Ground-based NRM is limited by atmospheric variability.

Optimization of space-based NRM requires consideration of flat fielding accuracy, target placement repeatability, charge diffusion, intrapixel sensitivity, image persistence, charge transfer efficiency, guiding, wavefront stability, pupil wander, and other details. We must assess NRM contrast limits realistically to understand the science yield of NRM in space, and, simultaneously, develop NRM science for planet and star formation and extragalactic science in the UV-NIR, to help steer high resolution space-based astronomy in the coming decade.

¹anand@amnh.org

Planetary system, star formation, and black hole science with non-redundant masking on space telescopes

1. Introduction

Major ground-based observatories have successfully implemented non-redundant aperture-masking interferometry using existing instruments and observing procedures. Landmark discoveries such as dusty disks imaged around young stellar objects, mass-loss shells of evolved stars, low mass companions to nearby stars, and the fascinating time-varying spiral plumes surrounding dusty Wolf-Rayet systems have been reported amongst the 50-odd peer-reviewed papers on NRM science (Tuthill et al. 1998; Monnier et al. 1999a,b; Tuthill et al. 2000, 2001, 2002, 2005, 2006; Lloyd et al. 2006; Pravdo et al. 2006; Martinache et al. 2007; Tuthill & Lloyd 2007; Ireland & Kraus 2008; Ireland et al. 2008; Tuthill et al. 2008; Martinache et al. 2008). However, atmospheric transmission and instabilities place significant limitations on ground-based non-redundant masking (NRM) performance. This will change with the advent of NRM on board space telescopes.

Detailed simulations of NRM performance on the *James Webb Space Telescope* (JWST) (Fig. 1) demonstrate the exciting planetary science enabled by the recent addition of NRM to JWST’s suite of established instruments, emphasizing the importance of this technique to other future space-based observatories (Sivaramakrishnan et al. 2009). On JWST NRM will widen the telescope’s science reach to include a unique combination of wavelength and angular resolution regimes inaccessible from the ground, even with the advent of extreme adaptive optics (ExAO) and coronagraphs behind 30 m extremely large telescopes of the future. NRM used at $4\ \mu\text{m}$ will bring within JWST’s purview warm extrasolar jovians within 4 to 30 AU of F, G, and K dwarfs 30 pc from the Sun (Fig. 2).

NRM adds high resolution capability to large filled-aperture space telescopes without sacrificing their wide utility for general astrophysical observations. The NRM search space is complementary to future coronagraphic space missions dedicated to extrasolar planet imaging and characterization (Kasdin et al. 2003), as well as to ground-based ExAO instruments (e.g. Macintosh et al. 2006), in that it yields moderate contrasts between 0.5 and $4\lambda/D$ (λ being the observing wavelength, D the telescope diameter). Diffraction-limited stellar coronagraphy, on the

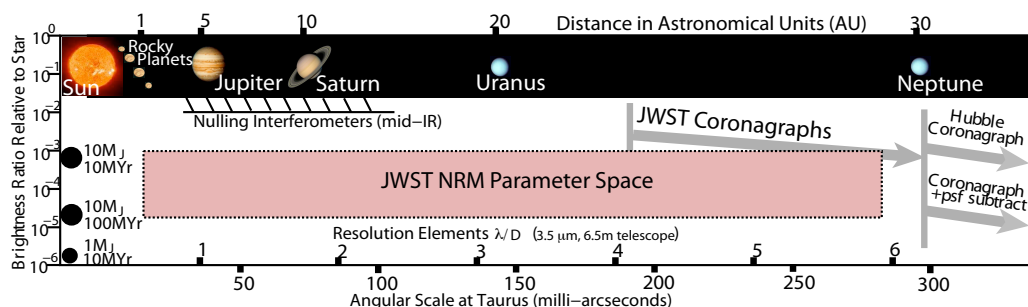


Fig. 1.— JWST FGS Tunable Filter Imager’s NRM search space.

other hand, typically covers a search space at higher contrast, but wider separations. Contrast-enhancing techniques such as Angular or Spectral Differential Imaging (e.g., Marois et al. (2006); Lafrenière et al. (2007) and references therein) are inefficient at the small angular separations covered by NRM.

Sivaramakrishnan et al. (2009) examined the scientific merit and feasibility of NRM on JWST FGS-TFI between $3.8\ \mu\text{m}$ and $5\ \mu\text{m}$, operating at a spectral resolution of 100 set by the étalon (NRM designs can perform just as well in 20% bandpass filters). The inner and outer working angles (IWA & OWA) of NRM scale with wavelength. CCD detectors in the visible/UV can be calibrated more accurately than JWST's IR focal plane arrays, resulting in improved NRM contrast.

2. NRM Interferometry and its limits

Interferometry with non-redundant baselines was initially developed for radio astronomy (Jennison 1958), and adapted to optical wavelengths (Baldwin et al. 1986). Today it is used in IR and optical bandpasses (Tuthill et al. 1998). A detailed description of NRM can be found in Haniff et al. (1989); Tuthill et al. (2000); Monnier (2003) and references therein. In brief, an N-hole pupil mask turns the extremely redundant full aperture of a telescope into a simpler interferometric array. Taking into account the geometry of the pupil (segmentation, central obscuration and spider vanes) as well as the spectral bandwidth, the mask is designed such that each baseline (a vector linking the centers of two holes) is unique: the mask is non-redundant in the sense that each spatial frequency is only sampled once (Fig. 3).

In a sense, NRM is a form of *imaging* with an unusual-looking PSF that displays multiple sharp peaks, whereas a traditional diffraction-limited PSFs is dominated by only one peak. However, the real virtues of the NRM PSF only appear after the image is Fourier transformed (e.g. Fig. 3 right panel): all spatial frequencies sampled by the mask appear as well separated peaks containing both amplitude and phase information. The advantages of this approach are that:

- The longest baseline provides a resolving power of $0.5\lambda/D$, compared to the traditionally accepted full aperture Rayleigh criterion limit of $1.22\lambda/D$.
- Unlike conventional PSF co-addition, dominated by a speckle noise floor (Sivaramakrishnan et al. 2002; Soummer et al. 2007a), the **information** extracted from the NRM data **can be averaged** to reduce noise, even in the presence of slowly-varying speckles.
- Non-redundancy ensures that the complex visibilities can be used to form **closure phases** (Baldwin et al. 1986), an observable that **calibrates** wavefront residual errors as well as **non-common path errors** between the science and sensing arms of the instrument.
- The outer working angle (OWA) is set by the shortest baseline, typically $4\lambda/D$: the **NRM** search space nicely **complements** that of **coronagraphy**.

It may seem perverse to throw away most of a telescope's collecting area, but the 10 – 20% mask transmission price paid for NRM (comparable to most high performance coronagraphs' throughput) purchases not only a straightforward $2.44\times$ gain in resolution but also a dramatic increase in signal to noise ratio. Today's ground-based NRM routinely achieves stability of 0.5

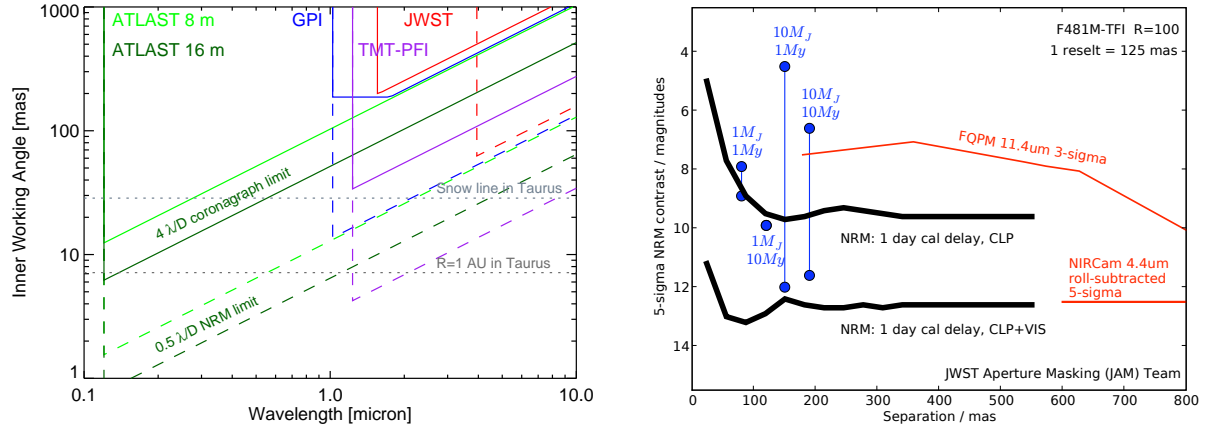


Fig. 2.— NRM and coronagraphy in space. *Left*: Solid lines show regions accessible with a $4\lambda/D$ inner working angle (IWA) coronagraph (e.g. JWST NIRCcam), while dotted lines mark the $0.5\lambda/D$ NRM limit. *Right*: Estimated dynamic range using closure phase (CLP) as well as closure phase and fringe visibility (CLP+VIS) data for 1% bandpass NRM imaging at $4.81 \mu\text{m}$ using the 7-hole mask (shown in Fig. 3) in JWST’s Fine Guidance Sensor’s Tunable Filter Imager. Protoplanets in Taurus will be detectable around an $M = 7$ star in a 10ks exposure, and a one day delay between the target and a calibrator star. Photon noise with this exposure limits the dynamic range to 10 magnitudes. The range of estimated contrasts between a solar type star and 1 and 10 Jupiter mass planets, at ages of 1 and 10 Myr (Baraffe et al. 2003; Marley et al. 2007) are shown in blue (at arbitrary separations). 10% bandwidths will produce similar results with 1ks exposures.

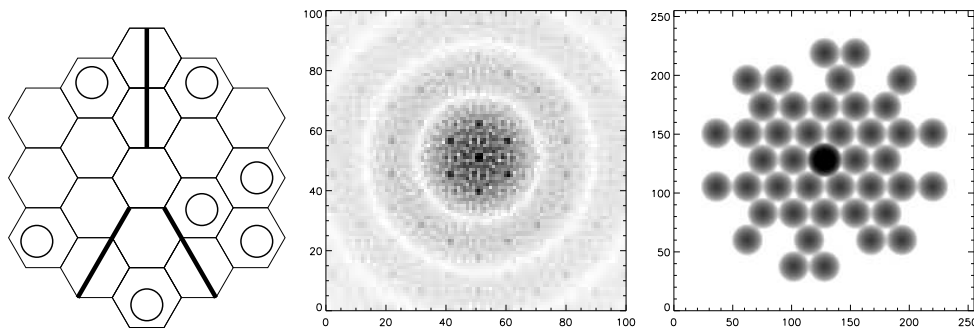


Fig. 3.— *Left*: A 7-hole non-redundant pupil mask (holes) overlaid on the JWST primary mirror. *Center*: A $4.05 \mu\text{m}$ FGS-TFI image of a point source, with a 1% bandwidth filter, on a negative logarithmic stretch (dark Airy rings appear white). The first Airy ring diameter is $2.4''$. Generally data out to the first Airy ring is analyzed. *Right*: the power spectrum of the image (also on a negative log scale), showing fringe power on the 21 baselines passed by the mask.

degrees on the closure phase, hence passively stabilizing the phase at the level of $\lambda/500$ to $\lambda/1000$, performance that will only be matched by the next generation of ExAO coronagraphic systems (Sivaramakrishnan et al. 2008).

Still, ground-based NRM suffers from rapid temporal instabilities due to atmospheric scintillation and transparency variations, as well as from differential atmospheric refraction. Space will provide an exceptionally stable environment that necessarily translates to increased performance. Space-based NRM contrast limits will then set by detector and telescope details: flat fielding accuracy, target placement repeatability, charge diffusion, intrapixel sensitivity, charge transfer efficiency, details of guiding and pupil wander, and the drift of the telescope structure due to slowly-varying thermal loads.

Accurate target placement on a detector can mitigate flat fielding uncertainties. Requirements on target placement and their relation to miscalibrated detector flat field responses must be derived from real CCD and NIR FPA detector data. Intrapixel sensitivity variations and charge transfer efficiency effects can be constrained with detector simulations (e.g. Sivaramakrishnan et al. 2003, 2004, see Fig. 4). Telescope stability and mechanical drift effect simulations already exist (Makidon et al. 2008), using ultrafine subpixel PSF generation (Soummer et al. 2007b). Finite element analysis (FEA) modelling of JWST (Lightsey et al. 2004) can incorporate breathing due to changes in the thermal environment of a segmented telescope, though monolithic 4 and 8 m space telescope should also be studied in the NRM context.

NRM filter bandwidths up to 20% are feasible. To utilize the performance capabilities of NRM fully it will be necessary to tackle two key tasks: first, the creation of realistic simulations of in-band/out-of-band spectral features such as methane, or emission/absorption lines around AGNs and GBHCs and, second, disk modeling for all types of astrophysical disks, with particular attention to predicted polarization. Although not attempted yet, polarimetric observations are perfectly compatible with NRM. The extra level of calibration added by polarimetry will translate into a higher overall sensitivity of the technique. Such high angular resolution polarimetry will require a sustained effort in disk modeling to develop strong science cases.

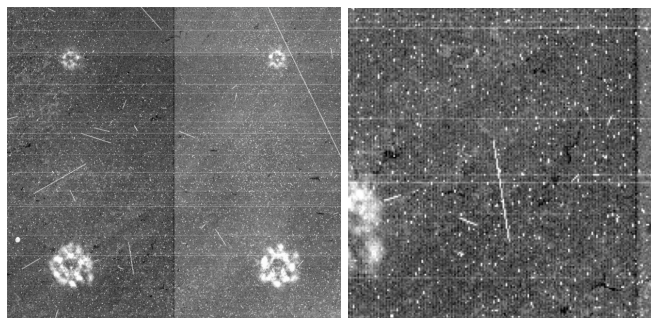


Fig. 4.— A JWST NIRCам HAWAII-2RG detector simulation using lab noise data (Sivaramakrishnan et al. 2003, 2004). *Left*: full detector. *Right*: section of detector. Realistic NRM data can be modelled similarly on IR Focal Plane Arrays (FPA) and CCDs.

3. Existing simulations and data analysis

Sivaramakrishnan et al. (2009) utilized a sample set of ten independent realizations of JWST's pupil within its wavefront error budget (Lightsey et al. 2004) to estimate the impact of mechanical drift on NRM contrast. JWST guiding errors and measured intra-pixel quantum efficiency were modeled to create images on the FGS-TFI pixel scale. Simulated data were analyzed with a pipeline used for Keck, Palomar, and VLT data. (e.g., Kraus et al. 2008). Nine of the ten PSF realizations in a set were taken to be calibrator observations, and one of the ten was taken to be the target observation. This process was repeated for several choices of target PSF. A pessimistic 5σ detection threshold was calculated, with closure-phase and visibility standard deviations estimated from the scatter within the 9 statistically independent calibrator observations. Fig. 2 (right panel) shows the contrast achieved with dynamic range calculated two ways: (1) using only the closure phases (labelled CLP) for a comparison with current ground-based results, and (2) using closure phases and fringe visibilities simultaneously (labelled CLP+VIS), to estimate the full range of contrast available to JWST. These methods need to be extended to cover the NIR to UV range, with adequately fine pixel sizes and anisotropic guiding errors, to illuminate the science role of NRM on proposed 4 to 16 m space telescopes.

4. Optical metrology and mission risk mitigation

In addition to its scientific merits, NRM can provide optical system metrology data with interferometric accuracy. A non-redundant array exhibits the remarkable property that each Fourier component in the image plane corresponds to a unique mapping to a pair of subapertures in the pupil. This mapping is an ill-posed problem for a full aperture. Direct metrology of the entire pupil can therefore be obtained with a finite number of simple measurements using the science detector.

This is particularly advantageous to any telescope with a segmented primary mirror. Every NRM image measures the relative mirror phase between each hole in the aperture mask, with a capture range set by filter coherence lengths; for a narrowband filter this can easily be several hundred microns. With measurements of the phase at multiple wavelengths (Martinache 2004; Borkowski et al. 2005), inter-segment piston can be measured to nanometer precision, starting from an initially disordered state. **No segment movement, defocus, or PSF degradation is required to perform wavefront sensing anywhere in the field of view: a mask in the science camera pupil suffices.**

Similarly, any science which requires a thorough understanding of temporal, field-dependent or chromatic PSF variations will benefit from precision metrology enabled by NRM. Thus NRM is a precise and flexible addition to the optical engineer's toolkit, providing unique diagnostics and mitigating mission risk.

5. Planet and star formation science with NRM in space

NRM's combination of very small inner working angle (IWA) with moderately high contrast opens the door to unique studies of star and planet formation inaccessible to other techniques. For example, the discovery that the transition disk surrounding CoKu/Tau4 T Tauri star is actually a

circumbinary disk was made with NRM at Keck (Ireland & Kraus 2008). Here we present only a few of the most exciting science cases enabled by space-based NRM.

An 8 m version of ATLAST with NRM would be sensitive to structure on scales as small as 1.3 mas for 0.1 μm , **almost an order of magnitude finer than ALMA’s finest resolution.**

EXTRASOLAR PLANETS AND CIRCUMSTELLAR DISKS: As mentioned above, aperture-masking on JWST will allow the detection of young planets around nearby stars in the thermal infrared (Sivaramakrishnan et al. 2009). There is justifiably great momentum for extending recent successes in coronagraphic imaging of exoplanets to higher contrasts in order to detect and characterize terrestrial planets. But it is just as important to understand the formation process(es) which lead to the observed diversity of exoplanets, a goal best accomplished by observing ongoing planet formation in protoplanetary disks on size scales similar to our solar system (0.3-30 AU).

The closest such disks can be found in nearby star forming regions such as Taurus and Ophiuchus at distances $d \sim 140$ pc. JWST NRM can potentially detect young planets there with separations > 12 AU. In Taurus, there are ~ 60 single stars with $M > 0.6 M_{\odot}$; a survey of the most promising 20 could require ~ 50 hours (see Fig. 2). NRM contrast should not degrade much for binary targets (unlike coronagraphy), so in theory NRM can probe a larger population of planets by targeting binary systems as well. However, further development of data analysis techniques for circumbinary planets is required before a major JWST survey is undertaken.

For future space telescopes, the improvement in IWA versus conventional coronagraphy brings within reach both previously unobservable regions of nearby systems as well as an increased survey space for more distant targets: NRM is able to observe targets in Orion with spatial resolution comparable to that achieved by coronagraphy for systems in Taurus (albeit at a lower contrast, but still one sufficient to detect luminous hot young giant planets). In conjunction with an 8-16 m space telescope, NRM may enable us to directly investigate how the properties of planetary systems vary with formation environment between loosely distributed T associations and the more massive OB associations.

Visible and near-UV observations with NRM on a ≥ 8 m space telescope offer the potential to detect structures such as gaps or spiral density waves on scales of 0.2–5 AU within disks in Taurus. Such observations directly probe the zones where terrestrial and Jovian planets are built, and will allow us to disentangle the relative contributions of planet formation models such as gravitational instability and core accretion (Kraus et al. 2009). Furthermore, they will let us observe planet/disk interactions to verify models for angular momentum transport and orbital migration.

Multiwavelength NRM imaging and polarimetry can be used to further constrain both disk structure and the nature of scattering bodies (Watson et al. 2007). For outer regions of disks accessible to existing coronagraphs (at separations > 30 AU), reflectance spectroscopy has been used to infer the presence of icy mantles on dust grains (e.g. Honda et al. 2009) and possibly even organic chemicals (Debes et al. 2008). NRM will, for the first time, extend such observations inward to the region of the “snow line” predicted around 4-5 AU (Fig. 2). Measurements of water ice absorption bands at 1.5, 2.0, and 3.1 μm will verify predictions of how particle properties vary across the snow line, directly relevant for planet formation models that posit buildup of

planetesimals at the snow line (Kretke & Lin 2007).

BIPOLAR OUTFLOWS are launched from disks in astrophysical contexts ranging from protoplanetary systems to supermassive black holes (e.g. Ray et al. 2007). Several theories have been advanced to explain their origin, but the physical mechanism(s) responsible for acceleration and collimation remain unclear. Discriminating between the various models requires spatially resolving the launch region (Ray et al. 2007; Ferreira et al. 2006), but the best observations to date (from HST STIS and AO integral field spectroscopy; Bacciotti et al. 2008 and references therein) are limited to resolutions of ~ 15 AU for the closest jets, compared to an inferred launch region size of ~ 5 AU (Hartigan et al. 2004).

NRM on an 8-m space telescope will be able to fully resolve the launching regions of jets from nearby YSOs, with a spatial resolution of ~ 1 AU at 656 nm for $d = 140$ pc. By observing jet opening angles and collimation scales, these observations will enable us to directly discriminate between disk and X-wind models. Such observations could be obtained using 1% wide filters, but NRM would be even more powerful in conjunction with a moderate-resolution optical integral field spectrograph, which would provide invaluable kinematic information as well as improved contrast by reducing the background of disk and star light against which jet emission lines must be detected. YSO jets in Taurus are the closest examples of collimated astrophysical outflows, and thus offer the best laboratory for detailed, high angular resolution study of the same physics which underlies jet production in systems as diverse as X-ray binaries and AGN.

6. Black hole environs science with NRM in space

Accretion flows around black holes (BH) cannot yet be imaged directly, rather we infer structure and composition from spectral information (e.g. McKernan et al. 2009 & references therein). For supermassive BH (SBH masses $\sim 10^6 - 10^9 M_\odot$), NRM will offer a direct view of critical parts of the accretion flow, providing a window on the nature and rate of mass supply to AGN, the orientation of the accretion flow around AGN, the accretion environment of low luminosity AGN (LLAGN) and will even permit a look at the kinematics of material as close as 80 AU to Sgr A*, the closest SBH. For Galactic black hole candidates (GBHC masses of few–few hundred M_\odot) space-based NRM will image their jets and accretion flows in unprecedented detail (0.6mas at $0.1\mu\text{m}$ or lengthscales of $\sim 1.2\text{AU}$ for Cyg X1).

SUPERMASSIVE BLACK HOLES: SBH live in the centers of galaxies, and can power AGN. Observed AGN properties are believed to depend on the orientation of the accretion flow to the observer’s sightline (Antonucci 1993) and its obscuration, with Type 1 AGN face-on and Type 2 edge-on to the observer. Space-based NRM imaging at 0.6–24mas together with polarimetry can provide unprecedented information on the orientation of the accretion disk, the disk outer structure (clumpy or smooth) and the AGN-host galaxy connection (for appropriate systems). NRM imaging resolution will be an order of magnitude finer than expected with ALMA (~ 5 –34mas at 0.5–3.6mm in the most extended 18km baseline configuration) (Maiolino 2008) or in preliminary coronagraphic studies of AGN ($\sim 70\text{mas}$) (Gratadour et al. 2005). With the addition of spectral information from a TFI or IFU we can map the kinematics of the accretion flow. A

JWST-TFI, has a kinematic resolution of $\sim 600 \text{ km s}^{-1}$ at $\sim 5 \mu\text{m}$, which will allow us to map the velocity field of the accretion disk and the Broad Line Region in Type 1 AGN.

NGC 1068 is the prototypical Seyfert 2 (Type 2) AGN, at a distance of 12.6 Mpc with $M_{\text{sbh}} \sim 10^7 M_{\odot}$ and a dusty torus $\sim 1.7 \text{ pc}$ ($\sim 17 \text{ mas}$) in radius (Jaffe et al. 2004). Space-based NRM imaging at 0.6-24 mas can probe the structure of the torus (internal heat sources, clumpiness), the narrow line region (NLR) clouds as well as the link between the outer edge of the torus and the host galaxy. Since the AGN phenomenon is believed to scale with SBH mass (e.g. McKernan et al. 2009 & references therein), an SBH 100 times more massive than that in NGC 1068 (i.e. $10^9 M_{\odot}$) could be probed at the same structural resolution as NGC 1068, at 10 times the distance ($\sim 126 \text{ Mpc}$). Lower luminosity AGN (LLAGN and LINERs) may be either highly obscured SBH or low accretion rate SBH. At $\sim 16 \text{ Mpc}$, NGC 3718 is classified as both a Seyfert 1 and a LINER with a central $M_{\text{BH}} \sim \text{few} \times 10^7 M_{\odot}$ and could be probed by space-based NRM (with a 16 m baseline) on scales of $\sim 0.05 - 2 \text{ pc}$, which spans the outer edge of the accretion disk and most of the dusty torus. In our own Galaxy, Sgr A* is an SBH ($\sim 3 \times 10^6 M_{\odot}$) with Schwarzschild radius of $\sim 0.1 \text{ AU}$ (Genzel et al. 2000) or $\sim 0.013 \text{ mas}$. At $\sim 2 \mu\text{m}$ NRM can probe to within $\sim 80 \text{ AU}$ of Sgr A* and monitor the motion of mass around a quiescent SBH on unprecedented scales.

BLACK HOLE GROWTH, AGN EVOLUTION AND COSMIC MERGER HISTORY OF GALAXIES: SBH mass seems to correlate with bulge luminosity and stellar velocity dispersion (i.e. elliptical galaxies and S0 galaxies tend to host larger mass SBH) (Kormendy & Richstone 1995; Magorrian et al. 1998; Ferrarese & Merritt 2000; Gebhardt et al. 2000; Barth et al. 2005; Greene & Ho 2006). If SBHs formed from the merger of earlier (possibly dwarf) galaxies, then the orientation of the accreting system should be random in large bulges and correlated with the host spiral galaxy orientation in galaxies with little or no bulge. NRM imaging combined with polarimetry will map AGN orientation with great accuracy, allowing us to test models of SBH growth and the host galaxy-SBH relation.

STELLAR MASS BLACK HOLES: GBHCs are the least luminous black holes, but because they are nearby, they are relatively easy to detect, usually as X-ray bright companions in X-ray binaries. The changing ‘states’ of GBHCs are believed to be caused by changes in the mass accretion rate, which triggers significant changes in the accretion flow geometry (Homan et al. 2001). Cyg X1, the original GBHC, is relatively typical at $\sim 2 \text{ kpc}$ distance and is separated from its companion by $\sim 0.2 \text{ AU}$ ($\sim 0.1 \text{ mas}$), with a period of ~ 5.6 days and a modulation period of ~ 142 days, possibly caused by accretion disk precession (Brocksopp et al. 1999). Cyg X1 has an intermittent relativistic radio-jet with an opening angle $< 2^\circ$ extending $\sim 15 \text{ mas}$ from the core (Stirling et al. 2001). At 0.1-4 μm , NRM resolution is 0.6-24 mas with a 16 m baseline which will reveal spectacular details in jet evolution and accretion outflows from close to the black hole. GBHC provide a laboratory to study the evolution of jets on timescales $\sim 10^{-6}$ faster than in AGN (Corbel et al. 2002).

7. Conclusion

Non-redundant aperture masking has established itself as a powerful and productive high angular resolution technique, and is implemented on most major ground based observatories. It was recently accepted as a late addition to JWST's FGS-TFI. There are good reasons: detailed simulations with time-varying mirror figure errors and existing data reduction methods suggest that non-redundant aperture masks would benefit any of the JWST instruments, bringing exciting high resolution high contrast imaging within reach. In fact, low cost, minimal impact on hardware, relaxed optical requirements, and high scientific payoff recommend NRM as a leading technology for any future missions possessing a high angular resolution imaging component.

8. Recommendations

- We recommend the development of a coronagraphy-NRM instrument for proposed 4, 8, and 16 m space telescopes at the Conceptual Design Review level. Scientific and technical trades between IFUs, tunable filters, or a filter wheel as spectral discriminators for NRM must be developed, with downselect at the end of 5 years. Detailed detector effects and telescope FEA results must be taken into account, and NRM data analysis methods developed further. [Cost: 5M\$, Time: 5 years]. This should be followed by systematic development of the chosen NRM design(s) [5M\$, 5 years].
- An exhaustive list of space-based NRM science opportunities, with exposure times and stability and hardware requirements, needs to be developed. Polarization must be an integral part of this effort. [1M\$, 5 years].
- Experimental verification and development of NRM, like other novel techniques, should be supported on existing ground-based telescopes and laboratory testbeds. [5M\$, 10 years].
- Early NRM work on Keck and Palomar provided a platform for the development of the ideas expounded here. Further ground-based observations with NRM should be supported to develop techniques and enhance the science return from future space-based NRM instruments and missions. [5M\$, 10 years].
- NRM is capable of sensing mirror phase to interferometric precision. We recommend its study and testing as a versatile, robust wavefront sensing system for future space telescopes, starting immediately with existing testbeds. [10M\$, 5 years].

REFERENCES

- Antonucci, R. ARA&A, 31, 1993, 473
- Bacciotti, F., McCaughrean, M., et al. In F. Bacciotti, L. Testi, & E. Whelan, eds., "Lecture Notes in Physics, Berlin Springer Verlag," vol. 742 of *Lecture Notes in Physics, Berlin Springer Verlag*. 2008, 151—
- Baldwin, J. E., Haniff, C. A., et al. Nature, 320, 1986, 595
- Baraffe, I., Chabrier, G., et al. A&A, 402, 2003, 701
- Barth, A. J., Greene, J. E., et al. ApJ, 619, 2005, L151
- Borkowski, V., Labeyrie, A., et al. A&A, 429, 2005, 747
- Brocksopp, C., Fender, R. P., et al. MNRAS, 309, 1999, 1063
- Corbel, S., Fender, R. P., et al. Science, 298, 2002, 196
- Debes, J. H., Weinberger, A. J., et al. ApJ, 673, 2008, L191
- Ferrarese, L. & Merritt, D. ApJ, 539, 2000, L9
- Ferreira, J., Dougados, C., et al. A&A, 453, 2006, 785
- Gebhardt, K., Kormendy, J., et al. ApJ, 543, 2000, L5
- Genzel, R., Pichon, C., et al. MNRAS, 317, 2000, 348
- Gratadour, D., Rouan, D., et al. A&A, 429, 2005, 433
- Greene, J. E. & Ho, L. C. ApJ, 641, 2006, L21
- Haniff, C. A., Buscher, D. F., et al. MNRAS, 241, 1989, 51P
- Hartigan, P., Edwards, S., et al. ApJ, 609, 2004, 261
- Homan, J., Wijnands, R., et al. ApJS, 132, 2001, 377
- Honda, M., Inoue, A. K., et al. The Astrophysical Journal Letters, 690, 2009, L110
- Ireland, M. J., Kraus, A., et al. ApJ, 678, 2008, 463

- Ireland, M. J. & Kraus, A. L. *ApJ*, 678, 2008, L59
- Jaffe, W., Meisenheimer, K., et al. *Nature*, 429, 2004, 47
- Jennison, R. C. *MNRAS*, 118, 1958, 276
- Kasdin, N. J., Vanderbei, R. J., et al. *ApJ*, 582, 2003, 1147
- Kormendy, J. & Richstone, D. *ARA&A*, 33, 1995, 581
- Kraus, A. L., Ireland, M. J., et al. *ApJ*, 679, 2008, 762
- Kraus et al. *Astro2010Whitepaper*:<http://www8.nationalacademies.org/astro2010/DetailFileDisplay.aspx?id=368>, 2009
- Kretke, K. A. & Lin, D. N. C. *ApJ*, 664, 2007, L55
- Lafrenière, D., Doyon, R., et al. *ApJ*, 661, 2007, 1208
- Lightsey, P. A., Barto, A. A., et al. In J. C. Mather, ed., “*Proc. SPIE*,” vol. 5487. 2004, 825–832
- Lloyd, J. P., Martinache, F., et al. *ApJ*, 650, 2006, L131
- Macintosh et al. In B. Ellerbroek and D. Bonaccini, ed., “*Proc. SPIE*,” vol. 6272. 2006
- Magorrian, J., Tremaine, S., et al. *AJ*, 115, 1998, 2285
- Maiolino, R. *New Astronomy Review*, 52, 2008, 339
- Makidon et al. In “*Proc. SPIE*,” vol. 7010. 2008, 70100
- Marley, M. S., Fortney, J. J., et al. *ApJ*, 655, 2007, 541
- Marois, C., Lafrenière, D., et al. *ApJ*, 641, 2006, 556
- Martinache, F. *Journal of Optics A: Pure and Applied Optics*, 6, 2004, 216
- Martinache, F., Lloyd, J. P., et al. *ApJ*, 661, 2007, 496
- Martinache, F., Rojas-Ayala, B., et al. *ArXiv e-prints*, 2008
- McKernan, B., Ford, K. E. S., et al. *MNRAS*, 394, 2009, 491
- Monnier, J. D. *Reports of Progress in Physics*, 66, 2003, 789
- Monnier, J. D., Tuthill, P. G., et al. *ApJ*, 525, 1999a, L97
- Monnier, J. D., Tuthill, P. G., et al. *ApJ*, 512, 1999b, 351
- Pravdo, S. H., Shaklan, S. B., et al. *ApJ*, 649, 2006, 389
- Ray, T., Dougados, C., et al. In B. Reipurth, D. Jewitt, & K. Keil, eds., “*Protostars and Planets V*,” 2007, 231–244
- Sivaramakrishnan, A., Lloyd, J. P., et al. *ApJ*, 581, 2002, L59
- Sivaramakrishnan, A., Makidon, R. B., et al. In J. C. Mather, ed., “*Proc. SPIE*,” vol. 4850. 2003, 388–397
- Sivaramakrishnan, A., Morse, E. C., et al. In J. C. Mather, ed., “*Proc. SPIE*,” vol. 5487. 2004, 909–917
- Sivaramakrishnan, A., Soummer, R., et al. *ApJ*, 688, 2008, 701
- Sivaramakrishnan et al. <http://olbin.jpl.nasa.gov/papers/preprint.html>, 2009
- Soummer, R., Ferrari, A., et al. *ApJ*, 669, 2007a, 642
- Soummer, R., Pueyo, L., et al. *Optics Express*, 15, 2007b, 15935
- Stirling, A. M., Spencer, R. E., et al. *MNRAS*, 327, 2001, 1273
- Tuthill, P., Monnier, J., et al. *Science*, 313, 2006, 935
- Tuthill, P. G. & Lloyd, J. P. *Science*, 316, 2007, 247
- Tuthill, P. G., Monnier, J. D., et al. *Nature*, 409, 2001, 1012
- Tuthill, P. G., Monnier, J. D., et al. *ApJ*, 624, 2005, 352
- Tuthill, P. G., Monnier, J. D., et al. In R. D. Reasenberg, ed., “*Proc. SPIE*,” vol. 3350. 1998, 839–846
- Tuthill, P. G., Monnier, J. D., et al. *PASP*, 112, 2000, 555
- Tuthill, P. G., Monnier, J. D., et al. *ApJ*, 577, 2002, 826
- Tuthill, P. G., Monnier, J. D., et al. *ApJ*, 675, 2008, 698
- Watson, A. M., Stapelfeldt, K. R., et al. *PPV*, 2007, 523